13th International Conference on
Structural Health Monitoring of Intelligent Infrastructure
DOI: 10.3217/978-3-99161-057-1-147

Intelligent Imaging: Transforming Concrete Assessment Methods with AI

A.Ahmad_,1,2 0000-0001-9427-4296, V.Plevris_3 0000-0002-7377-781X M.ullah_3 0000-0002-7212-8826 and J.Mir_4 0000-0002-4587-5121
[1]Department of Built Environment, Oslo Metropolitan University, Oslo, Norway
[2]Civil Engineering Department, University of Memphis, USA
[3]Department of Civil and Environmental Engineering, Qatar University, Qatar
[4]Department of Electrical Engineering, University of Engineering & Technology, Taxila, Pakistan

*Email: afaq.ahmad@oslomet.no

ABSTRACT: This study uses novel image processing techniques to explore the effects of Cement Replacement Materials (CRM) like silica fume and fly ash on concrete's microstructure and durability. Cylindrical concrete specimens were prepared with mixed ratios of 1:2:4 and 1:3:6, incorporating water-cement (W/C) ratios of 0.4, 0.5, and 0.6 and CRM levels of 0%, 15%, and 25%. Images captured at various cylinder heights were analyzed using rectangle and nearest neighboring methods to quantify aggregate distribution and air void characteristics, including area, size, and spacing. Validation against manual measurements showed an error rate of less than 1.9%, underscoring the accuracy of these techniques. Results indicated that increasing CRM content reduced air void proportion and size, indicating improved durability. Additionally, CRM increased concrete homogeneity, with 25% of CRM samples exhibiting the lowest coefficient of variation (Cv) values (0.29–0.37), compared to higher Cv values (0.41–0.57) in non-CRM mixes. These findings highlight CRM's potential to enhance concrete mix design for better structural performance and sustainability in construction applications.

KEY WORDS: CRM, Concrete, Image Processing

1 INTRODUCTION

Concrete holds significant importance in civil infrastructure construction due to its favorable properties such as durability, strength, adaptability, and ease of availability. Concrete consists mainly of cement, aggregates, and water, making it a composite material. The cement paste, formed by mixing water with hydraulic cement, acts as a binding agent in concrete formulations. Cement is the most expensive component within the concrete matrix. Moreover, the escalating global demand for cement production contributes to the upward trend in environmental CO2 levels [1]. To reduce both the economic and ecological impacts associated with cement production, the incorporation of cement replacement materials (CRMs) has gained prominence, leveraging waste materials like silica fumes (SF) and fly ash (FA) as viable alternatives to conventional cement [2, 3]. CRM can significantly affect the rheology of the mortar, which refers to its flow properties [4, 5]. FA particles are fine and spherical and act as ball bearings, reducing internal friction between cement particles and making the mix more workable in the concrete mixture [6]. SF particles are extremely fine with a high surface area, which enables them to fill the spaces between cement particles and create a dense matrix. This results in increased viscosity and reduced flowability in the concrete [7]. Therefore, aggregate distributions and air void content in concrete are affected by CRM due to the changes it induces in the rheological and microstructural properties of the concrete [8].

The distribution of aggregates and air voids in concrete offers valuable insights into the concrete sedimentation behavior, directly impacting its stability, structural serviceability, durability performance, and resistance to cracks [9, 10, 11]. Concrete petrographic analysis (ASTM C856) [12] is a commonly utilized method for assessing many concrete aspects, e.g., size and distribution of aggregates, porosity levels, and bughole formations etc. [13]. Typically, concrete petrography entails the micro-structural examination of concrete components on a polished concrete section using imaging methods such as optical microscopy [14] or scanning electron microscopy [15]. In the past, human experts have conducted petrographic analysis by visually inspecting bugholes and aggregate distribution in cut sections of hardened concrete to evaluate its stability [16]. Determination of the size of aggregate particles has traditionally been done through mechanical sieving or manual clippers, but these methods are susceptible to human bias, errors, monotony, and inefficiency. Hence, there is a growing need for automated techniques and alternative methods to assess concrete stability.

In recent years, digital image processing has emerged as a widely employed tool in structural health monitoring (SHM) of concrete structures. [17]. Numerous studies have leveraged image processing techniques for the distribution analysis of aggregates within concrete. Aggregate size, area, and distribution within the concrete mixture are assessed to investigate the stability of self-compacting concrete [18]. Characteristics and distribution of coarse aggregate were computed in [19] by segmenting the concrete image into the background (cement paste) and foreground (aggregates). Characteristics and distribution of coarse aggregate are evaluated in [20] by an image analysis method using cross-sectional images. The consistency between 3D and 2D parameters is assessed, and a comparison of the ratio of mortar-to-coarse aggregate area with the mortar-to-coarse aggregate volume is presented. The aggregate distribution analysis in asphalt concrete was carried out by examining the aggregates' segmented images obtained through X-ray computed tomography in [21]. An aggregate classification approach that considers mesoscale angularity is proposed in [22].

DOI: 10.3217/978-3-99161-057-1-147

This paper presents image processing-inspired techniques for assessing the impact of CRM on the concrete characteristics i.e., aggregate distribution, air void formation, and mixture homogeneity and segregation. To ameliorate this, concrete cylinders of different mix design ratios and percentages of SF and FA cut at the top and bottom sections were imaged to capture the internal concrete characteristics. Then, the images were annotated with pixel-level labels to facilitate quantitative analysis. Image processing-based methods are presented for aggregate and air void analysis to understand the impact of different CRM ratios in a concrete mixture. Subsequently, indicators for assessing concrete homogeneity are introduced by integrating aggregate size, roundness, and inter-aggregate distances. The study provides valuable insights into the segregation of aggregates and air void proportions within the concrete mixes and provides a comprehensive understanding of the sedimentation behavior induced by CRM.

2 DATABASE

2.1 Preparing Concrete Mixtures:

Two distinct designs of concrete were chosen, each with different proportions of cement, fine aggregates, and coarse aggregates for casting. These proportions were specified as 1:3:6 and 1:2:4. Mixes were formulated using different W/C ratios (0.4, 0.5, and 0.6) under the standards set by ASTM C 94 [23] and ACI 318 [24], since the variability in the water/cement (W/C) ratio plays a significant role in influencing the workability and distribution of aggregates within concrete. A total of six mix designs were included in the cast samples. Fly ash (FA) and silica fume (SF) were employed as Cement Replacement Materials (CRM) at varying replacement percentages of 0%, 15%, and 25% to assess their impact on the distribution of aggregate and air voids within the concrete mixtures. Two batches of 18 concrete cylinders were produced using the mix design ratios outlined in Table 1, and were allowed to cure for 14 and 28 days, respectively. These cylindrical samples were 300 mm in height (H) and 150 mm in diameter (D). They were then cut into three slices at 1/3rd and 2/3rd sections (approximately 100 mm from the bottom and top) using a stone cutting saw. The cutting procedure for acquiring concrete slices is depicted in Figure 4. Due to the fine materials accumulation on the bottom face of the third slice, and the top face of the first slice had minimal or no aggregate information and were thus excluded from imaging. This left four faces for imaging to generate the dataset.

Table 1. Detail of the samples with Mix Ratios

Sr. No.	Mix Ratio	W/C Ratio	FA %	SF %	Proportions in kg/m^3					
					Cement	FA	SF	Find Aggr.	Coarse Aggr.	Water
1	01:03:06	0.4	0	0	229.48	0	0	728.94	1505.78	91.8
2	01:03:06	0.5	0	0	229.48	0	0	728.94	1505.78	114.75
3	01:03:06	0.6	0	0	229.48	0	0	728.94	1505.78	137.69
4	01:02:04	0.4	0	0	327.79	0	0	694.27	1434.06	131.12
5	01:02:04	0.5	0	0	327.79	0	0	694.27	1434.06	163.9
6	01:02:04	0.6	0	0	327.79	0	0	694.27	1434.06	196.68
7	01:03:06	0.4	15	15	160.64	34.43	34.43	728.94	1505.78	91.8
8	01:03:06	0.5	15	15	160.64	34.43	34.43	728.94	1505.78	114.75
9	01:03:06	0.6	15	15	160.64	34.43	34.43	728.94	1505.78	137.69
10	01:02:04	0.4	15	15	229.45	49.18	49.18	694.27	1434.06	131.12
11	01:02:04	0.5	15	15	229.45	49.18	49.18	694.27	1434.06	163.9
12	01:02:04	0.6	15	15	229.45	49.18	49.18	694.27	1434.06	196.68
13	01:03:06	0.4	25	25	114.75	57.38	57.38	728.94	1505.78	91.8
14	01:03:06	0.5	25	25	114.75	57.38	57.38	728.94	1505.78	114.75
15	01:03:06	0.6	25	25	114.75	57.38	57.38	728.94	1505.78	137.69
16	01:02:04	0.4	25	25	163.9	81.95	81.95	694.27	1434.06	131.12
17	01:02:04	0.5	25	25	163.9	81.95	81.95	694.27	1434.06	163.9
18	01:02:04	0.6	25	25	163.9	81.95	81.95	694.27	1434.06	196.68

The image acquisition setup was organized in a closed room, depicting an experimental arrangement for capturing digital images of concrete specimens, as shown in Figure 1.To ensure high-quality images for effective processing, measures were taken to maintain a consistent environment and minimize external influences such as light variations, noise, and shadows. Black sheets were used to cover all entry points for light, and two 30-W LED bulbs provided controlled illumination from a specific angle, resulting in a light intensity of 2000 lux. A digital camera (Nikon DSLR 3300) with a resolution of 24 megapixels and ISO value set at 1000 was employed to capture 192 high-resolution slice images, each measuring 6000→4000 pixels. A constant distance was maintained by mounting the camera on a stand at a distance of 600 mm from the surface of the sample. The image acquisition setup, for example slice image, is illustrated in Figure 1.

DOI: 10.3217/978-3-99161-057-1-147

Figure 1. Preparation of Concrete Mixtures (Top Left), Casting and Cutting of Samples (Top Right), Image Acquisition (Bottom Left), Image Labeling (Bottom Right).

2.2 Casting and Cutting of Samples

Two batches of 18 concrete cylinders were produced using the mixed design ratios outlined in Table 1, and were allowed to cure for 14 and 28 days, respectively. These cylindrical samples were 300 mm in height (H) and 150 mm in diameter (D). They were then cut into three slices at 1/3rd and 2/3rd sections (approximately 100 mm from the bottom and top) using a stone cutting saw. The cutting procedure for acquiring concrete slices is depicted in Figure 2. Due to the fine materials accumulation on the bottom face of the third slice, the top face of the first slice had minimal or no aggregate information and was thus excluded from imaging. This left four faces for imaging to generate the dataset.

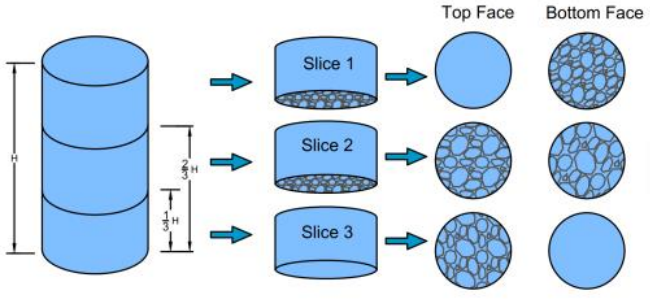

Figure 2. Cutting the concrete cylinders into three slices at top and bottom sections

2.3 Image Labeling

Each image was meticulously labeled at the pixel level to distinguish between non-aggregate suspension (e.g., air voids, sand-cement matrix) and aggregate pixels. Similarly, for air void analysis, image pixels were labeled as either air void pixels or non-air void suspension pixels (e.g., aggregates, sand-cement matrix). Binary images were generated for aggregates and air voids, respectively.

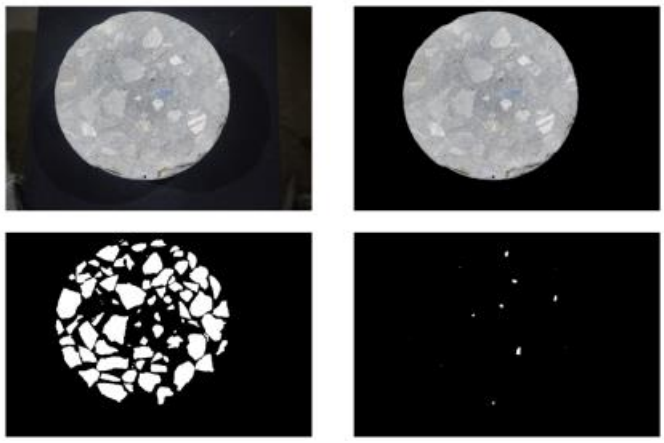

Figure 3. High-resolution images of concrete slices: The top left is the original image, the top right is the background removed image, the bottom left is the Aggregate ground truth and the bottom right is the Air void ground truth image

Figure 3 shows a concrete cylinder slice with background, the processed image with the background removed, and the corresponding ground truth images for aggregates and air voids. White pixels in these images indicate the presence of aggregates and air voids as per the ground truth labels. Among all the labeled pixels across 144 slice images, 41.3% were labeled as aggregate pixels and 58.7% as non-aggregate pixels. Similarly, 0.25% of labeled pixels were labeled as air void pixels, with 99.75% classified as suspension pixels. Among all the labeled images, 1.8% of the particles were found to be connected. On average, each connected component consisted of approximately 13 pixels. These connected components were separated with a Marker-controlled watershed transformation algorithm [25] enabling detailed analysis and quantification of characteristics of each aggregate and air void in concrete samples.

DOI: 10.3217/978-3-99161-057-1-147

The aggregates and air voids proportions can significantly influence the rheology, stability, mechanical characteristics, durability, and cost-effectiveness of concrete. These proportions can be determined from annotated images. The overall area occupied by aggregates and air voids in a concrete cylinder was determined by counting the white pixels, representing aggregates and air voids, and then multiplying it by the unit pixel size. Then this pixel size is converted to 0.044 mm. To validate this method, the aggregate and air void characteristics were compared with measurements obtained manually and using AutoCAD [26]. For manual area measurement of aggregates and air voids, a transparent graph paper with a 1 mm square grid was placed on the cylinder surface to count squares covering aggregates and air voids, as illustrated in Figure 4. The numbers of squares fully and partially covering aggregates and air voids were counted and then finally summed to determine the area of aggregate and air void, respectively. The aggregate mean size and roundness values were manually verified against a vernier caliper, as illustrated in Figure 4. In AutoCAD [26], the raster images were first scaled according to the standard diameter of the cylinder. Subsequently, the boundaries of the aggregates and air voids were then traced, and certain boundary points were marked to form polygons, as depicted in Figure 4. With the help of a built-in command, the area of these polygons was calculated based on the coordinates of the boundary points. This approach differs from the pixel-based method, enabling a meaningful comparison between the two techniques. The areas of these polygons were then summed to determine the total aggregate and air void area, respectively. A comparison of aggregate and air void characteristics measured using the proposed image processing method, manual measurements, and AutoCAD is presented in Table 2. The results demonstrate significant consistency, confirming the effectiveness of the proposed image processing method in precisely identifying characteristics of aggregates and air voids.

Table 2. Comparison of the computed areas

Parameters	**Mix Ratio**	**Proposed Method**	**AutoCAD**	**Visual Inspection**	**Percentage Error**
Aggregate Area (mm^2)	01:02:04	9335.35	9297.12	9411.25	0.81
	01:03:06	10058.42	10083.88	10171.5	1.11
Aggregate Mean Size (mm)	01:02:04	14.84	14.53	14.75	0.61
	01:03:06	15.36	15.64	15.5	0.9
Aggregate Mean Roundness	01:02:04	1.73	1.81	1.75	1.14
	01:03:06	1.52	1.43	1.5	1.33
Air-voids Area (mm^2)	01:02:04	5.19	5.31	5.25	1.14
	01:03:06	9.68	10.12	9.5	1.89
Air-voids Mean Size (mm)	01:02:04	2.53	2.42	2.5	1.2
	01:03:06	2.77	2.87	2.75	0.73

2.4 Aggregate and Air Void Characteristics:

An object's characteristics, like size, shape, and orientation, can tell much about its concrete composition. Quantifying these characteristics can lead to size and distribution uniformity analysis, which in turn facilitates the examination of concrete mixture's consolidation, workability, compatibility, interlocking, and bonding. The Feret rectangle technique [27] was utilized in this study to measure the characteristics of the coarse aggregate and voids from the image. This technique entails drawing rectangles that enclose each object with the minimum area possible, according to their Feret diameter as depicted in Figure 5. The Feret diameter represents the greatest distance between points along the object's perimeter. To compute this, we iterated through pairs of points on the boundary line, calculating their Euclidean distances and identifying the greatest distance as the Feret diameter. Subsequently, around each object, a rectangle was drawn, with its length corresponding to the Feret diameter and its width perpendicular to this direction. The orientation of these rectangles was optimized to minimize their area while encompassing the object. The dimensions, i.e., length and width of each Feret rectangle, were then determined and recorded as the corresponding object's length and width. The length of the object was considered as its size, and the mean aggregate size was calculated as the average of all aggregate sizes measured in the image. The roundness values of coarse aggregates were assessed by computing the ratio of the rectangle's longer side to its shorter side. A roundness value of one signifies a square-shaped rectangle. As the roundness increases, the shape of the object becomes more elongated.

DOI: 10.3217/978-3-99161-057-1-147

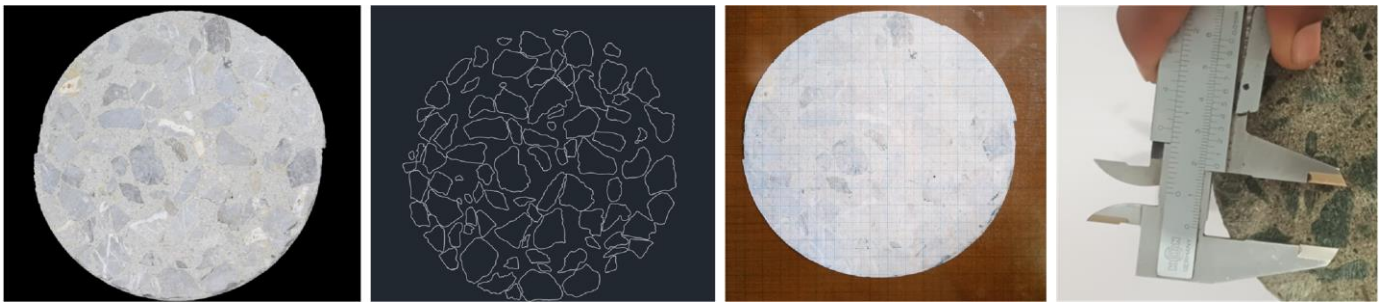

Figure 4. Concrete sample (1st image), traced boundaries using AutoCAD (2nd image), manual area measurements with graph paper (3rd image), and manual size measurement with vernier caliper(4th image)

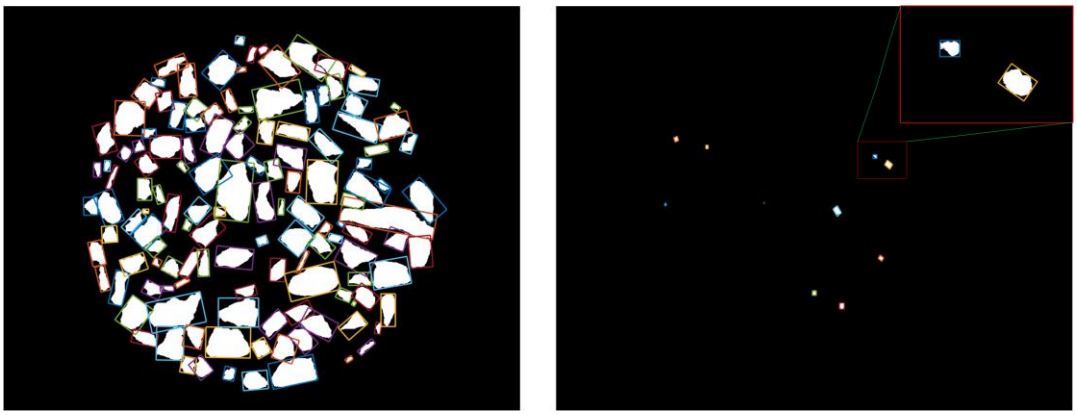

Figure 5. Concrete sample image showcasing minimum area rectangles derived from Feret diameter; Aggregate (Left), Air void (Right).

3 RESULTS AND DISCUSSION

3.1 Aggregate Proportion

The proportion of aggregate in the concrete mixture is an essential factor in analyzing the structural health of a member and can be calculated using the image processing methodologies discussed previously. As presented in Table 1, in this study, two mix ratios, 1:2:4 and 1:3:6, were employed. These mix ratios denote the proportions of cement, fine aggregates (sand), and coarse aggregates in 1 m3 volume of concrete. Initially, the proportion of coarse aggregates in the cylinder was quantified using the aggregate volume ratio (AVR) parameter. AVR represents the ratio of coarse aggregate volume to the total volume of a cylinder, as given by Eq. 1,

$$AVR = \frac{Coarse\ Aggregate\ Volume}{Cement+Sand+Coarse} \quad (1)$$

According to Eq. 1, the mix ratios of 1:2:4 and 1:3:6 correspond to AVR values of 0.57 and 0.60, respectively. The AVR values were then compared with the proportions of aggregates obtained from 2D cross-sectional images of the cylinder. By analyzing concrete cross-sectional images and computing areas of aggregate, the proportion of aggregates in 2D images was quantified using the aggregate area ratio (AAR), given as Eq. 2,

$$AAR = \frac{Area\ of\ Aggregate\ in\ Image}{total\ cross\ scetional\ area\ of\ cylinder} \quad (2)$$

Here, the total cross-sectional area of the cylinder refers to the area encompassed by all pixels within the cylinder boundary. Figure 6 illustrates the AAR values obtained from the cross-sectional images for the two mix ratios across different CRM ratios. An observable trend emerges where an increase in the CRM ratio corresponds to a reduction in the variation of deducted AAR values. This may be because the incorporation of CRM results in a more uniform distribution of aggregates in concrete compared to normal concrete. It is noticeable that the calculated AAR values exhibit deviation from the AVR values. The disparity in AAR values may arise from several factors. Segregation can occur during mixing, transporting, and casting of concrete, leading to a nonuniform distribution of aggregates within concrete. These factors directly influence the calculated AAR values.

DOI: 10.3217/978-3-99161-057-1-147

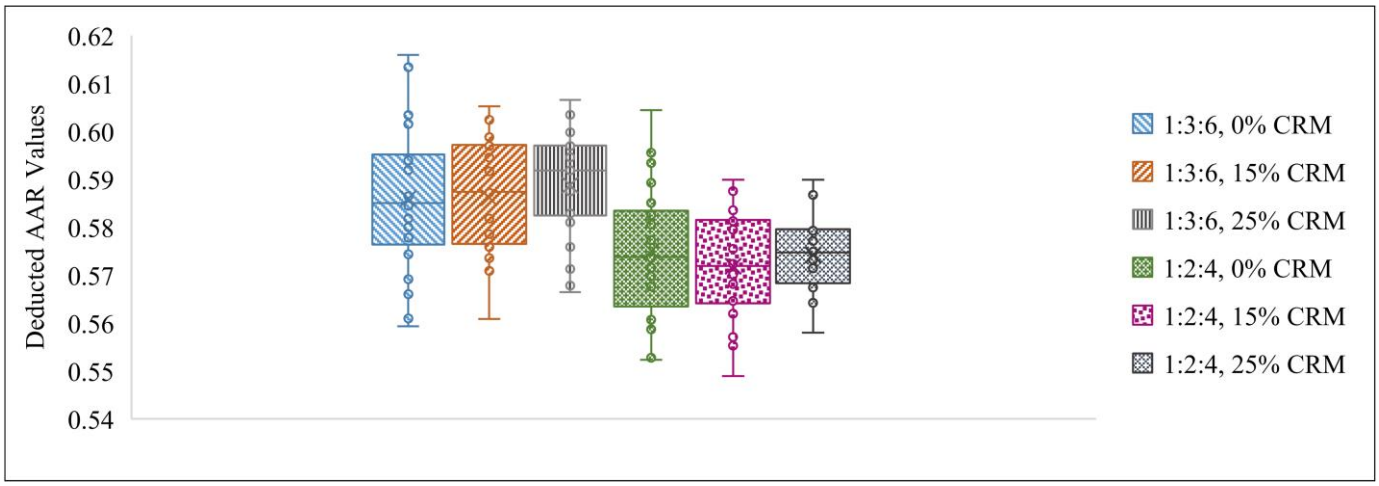

Figure 6. Box-Plots showing variation of calculated AAR values for the two mix designs with varying CRM ratios.

3.2 Aggregate Size

In segregation, the coarser aggregate particles tend to settle down, and the finer aggregate particles remain at the top. The sizes of aggregates at the bottom and top regions of concrete cylinders were analyzed (as detailed in Section 2.2) to assess the impact of different proportions of W/C ratio and CRM on segregation. Analysis of aggregate size involves examining cross-sectional images of the concrete cylinder at the top region (comprising the bottom face of the first slice and top face of the second slice) and the bottom region (comprising the bottom face of the second slice and top face of the third slice). The difference in aggregate mean size between these regions indicates the extent of segregation and is shown in Figure 7 for different CRM Ratios. Within each mix ratio (1:2:4 and 1:3:6), generally, there is a slight increase in the difference in mean aggregate size with an increase in W/C ratio, which indicates the occurrence of segregation. This occurs because higher water content increases the mobility and fluidity of the concrete mix, making it more susceptible to segregation during handling, transportation, or placement. Excessive water can cause coarser particles to settle, increasing the size disparity between the aggregates.

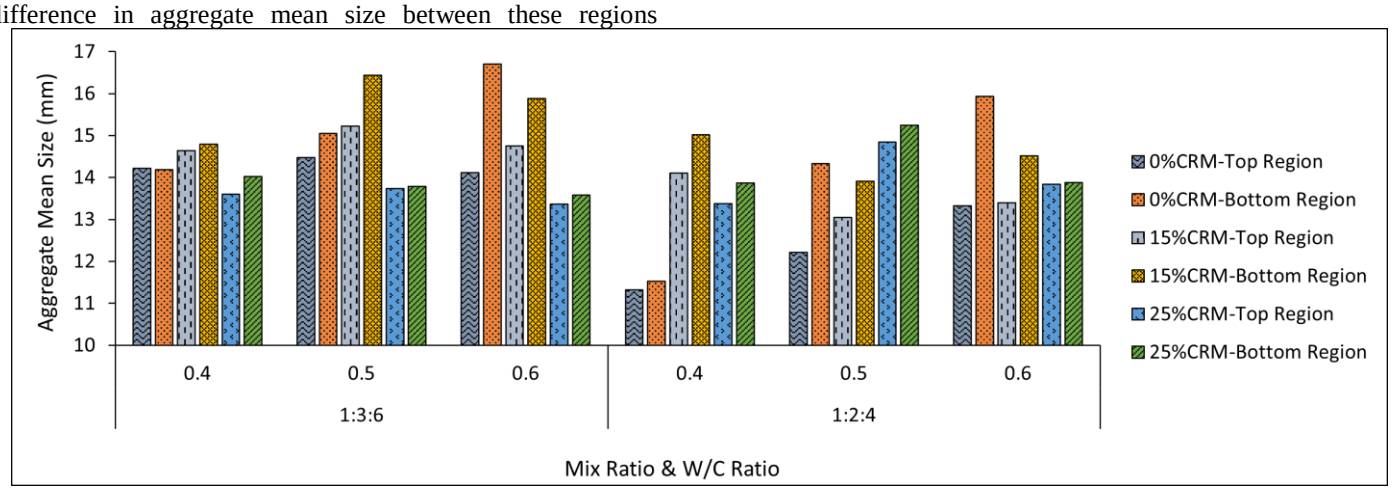

Figure 7. Mean size of coarse aggregates at bottom and top regions of the concrete cylinders bottom and top regions.

3.3 Aggregates Roundness

The roundness of aggregates significantly influences segregation in concrete. Less rounded aggregates have irregular shapes with sharp edges and corners. When these less-rounded particles come in contact, they interlock, creating a bridging effect in the concrete mix. This bridging effect minimizes the risk of segregation for the less-rounded particles. On the other hand, more rounded aggregates have a uniform shape, making them less prone to interlocking and bridging. This can result in a higher likelihood of particle movement and segregation within the mix. The more rounded shape reduces the frictional forces between particles, allowing them to move more freely and potentially separate from one another. The mean roundness values of aggregates in the top and bottom regions of the concrete cylinders are calculated using a specified method. Figure 8 represents the analysis results of aggregate mean roundness values at the bottom and top regions of a concrete cylinder with 0%, 15%, and 25% CRM, respectively.

DOI: 10.3217/978-3-99161-057-1-147

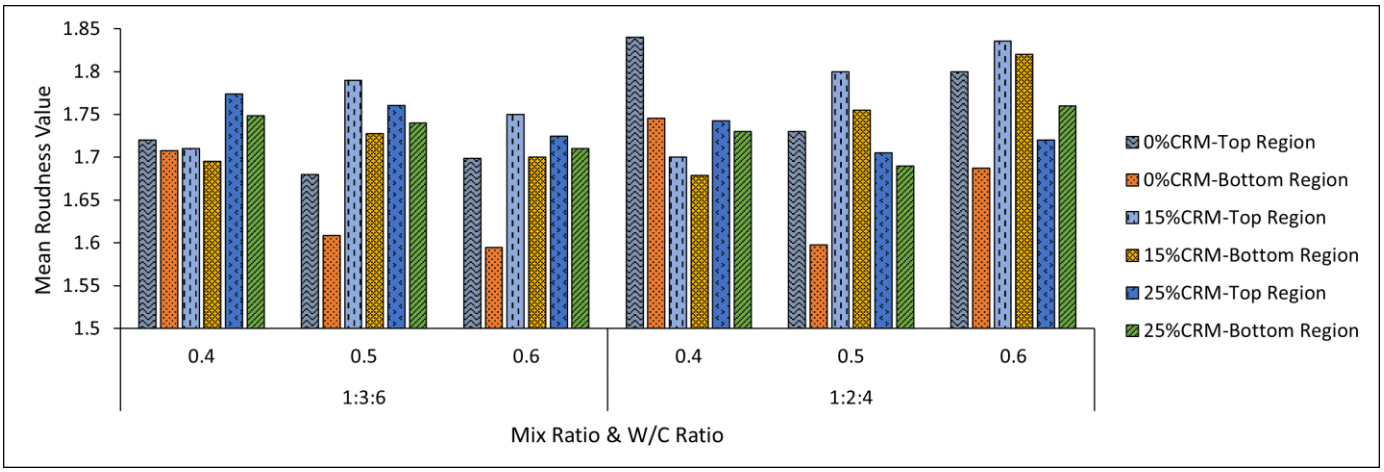

Figure 8. Mean roundness values of coarse aggregate at bottom and top regions of the concrete cylinders.

3.4 Distance Between Aggregates

The examination of the distribution of aggregates in the bottom and top regions of concrete specimens can provide valuable information about the concrete sedimentation behavior. To examine the effect of CRM and W/C ratios on the distribution of aggregates, the distance between centroids of coarse aggregate particles was determined by the nearest neighbor image analysis method. The frequencies of these distances for different range groups are then determined for each section. Figure 9 shows the frequencies of distances between the aggregate for the specified range groups at different CRM and W/C ratios. The frequencies of distances between coarse aggregates are shown separately for the bottom and top regions of the concrete cylinder specimens. Most aggregate distributions fall within the 10 mm- 20 mm distance range in all specimens. Notably, the 0% and 25% CRM cylinders exhibit a high frequency within the range of 10 mm- 20 mm spacing distances, indicating closer aggregate spacing compared to the 15% CRM specimens. Figure 13 also reveals that the frequency of distances between 10mm and 20mm is higher in the bottom region, suggesting a more compact arrangement of aggregates at the bottom. Additionally, the frequency of distances within the range of 30 mm- 40 mm and 40 mm- 50 mm is lower in the bottom region compared to the top region. This difference can be attributed to the settlement of heavier aggregate particles, which results in closer spacing of aggregates within the 10 mm- 20 mm range, consequently reducing the maximum spacing between aggregates, typically in the 30 mm- 50 mm range.

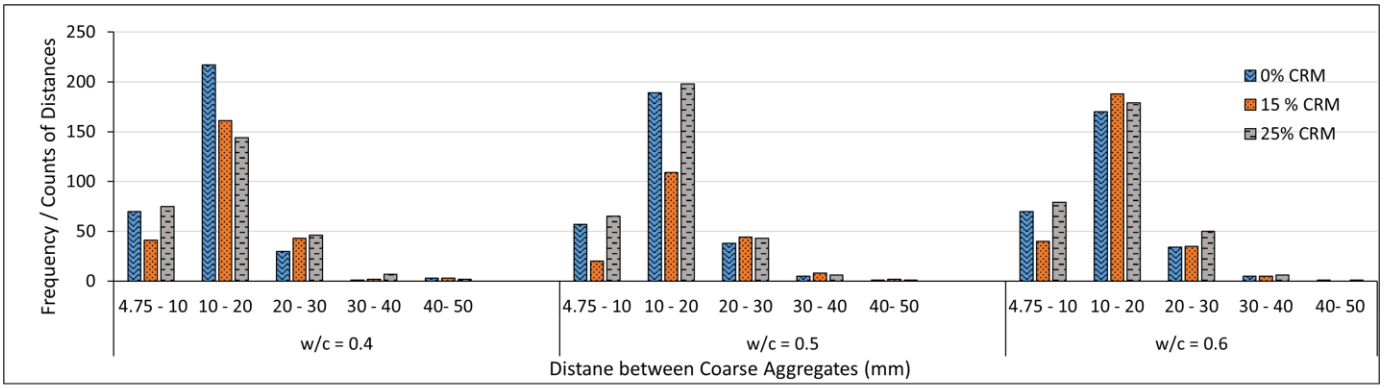

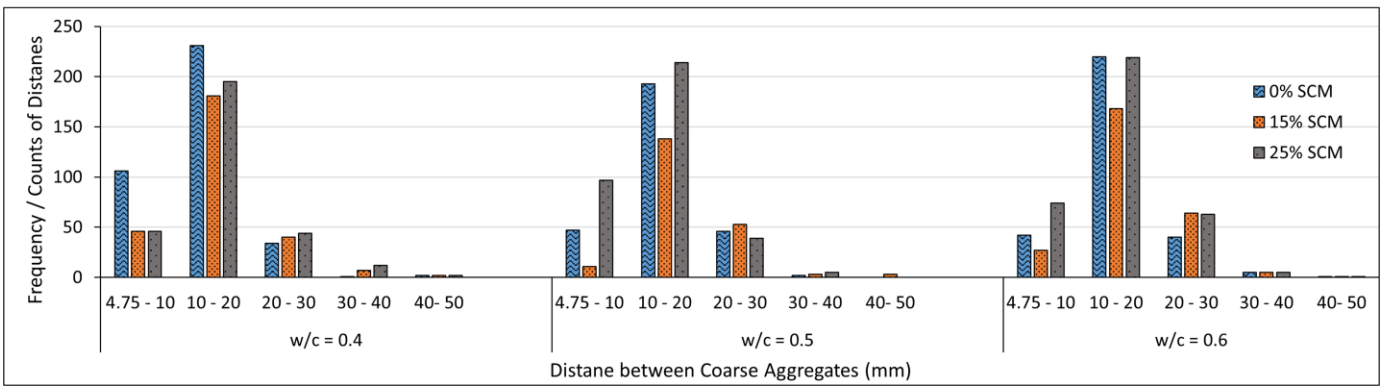

DOI: 10.3217/978-3-99161-057-1-147

Figure 9. Frequency of distances between centriods of coarse aggregate particles; Top Cylinder Region (First row), Bottom Cylinder Region (Second row)

3.5 Air Void Proportion

Assessing the air void proportion within a concrete mixture is a crucial step for achieving the desired balance between durability and mechanical properties, and it can be determined using the image analysis techniques described above. The air void proportion in the 2D cylinder images was quantified through the area air void ratio (AAVR) parameter, which is calculated as Eq 3.

$$AAVR = \frac{area\ of\ air\ void\ in\ image}{total\ cross\ scetional\ area\ of\ cylinder} \quad (3)$$

Here, the total cross-sectional area of the cylinder slice refers to the area encompassed by all the pixels contained within the boundary of the Concrete cylinder. Figure 10 displays the AAVR values computed from the images of concrete cylinder specimens for the two mix ratios with varying CRM ratios. Across varying W/C ratios and concrete mix ratios, a consistent trend emerges. Generally, as the percentage of CRM increases from 0% to 15% and 25%, the proportion of air voids tends to decrease. This suggests that incorporating CRM, such as FA or SF, can reduce the formation of air voids in concrete. This reduction in AAVR values can be attributed to the pozzolanic properties of FA and SF, which enhance the workability and cohesion of the concrete mix, reducing the likelihood of entrapped air and thus decreasing the number of air voids. These findings offer valuable insights into optimizing concrete mix designs with CRM to minimize air voids. It's also worth noting that the W/C ratio effects the influence of CRM on air void proportion, as the two factors interact to shape the entrapped air content, highlighting the importance of considering both factors when optimizing concrete mix designs for specific applications.

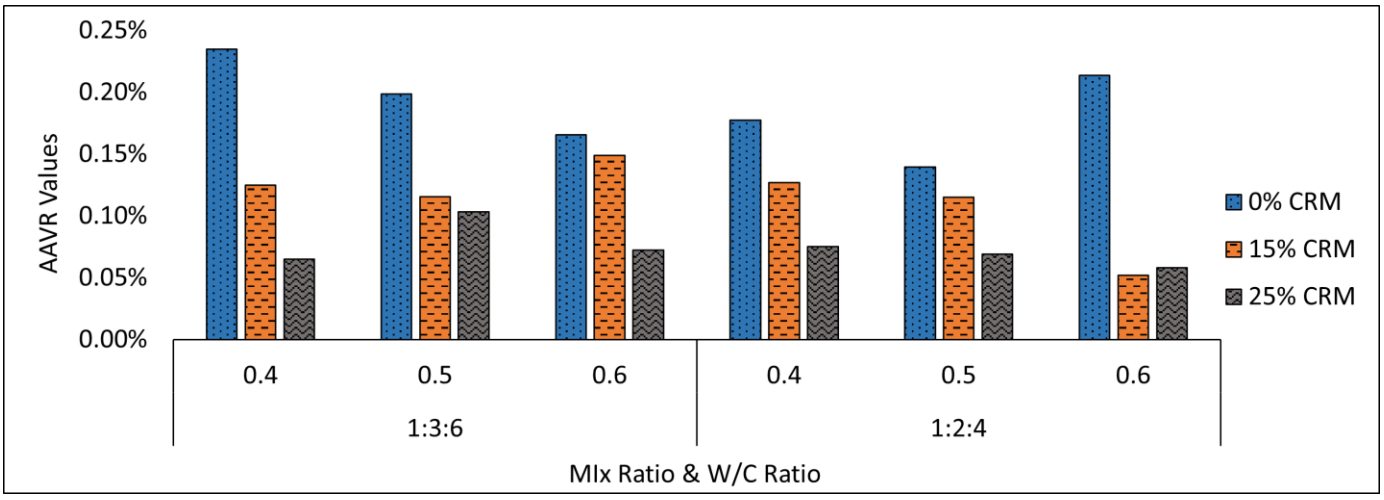

Figure 10. Influence of CRM on the area air void ratios

3.6 Air Void Size

The size of air voids significantly impacts concrete properties. Smaller air voids enhance the concrete's resistance to freeze-thaw cycles, enhancing durability. Larger air voids, on the other hand, can weaken the concrete's mechanical properties, making it more vulnerable to cracking and deterioration in challenging environmental conditions. Achieving the right balance in air void size is crucial in optimizing concrete for specific applications, ensuring a combination of strength, durability, and long-term performance. To understand the effect of different CRM and W/C ratios on the size of air voids, the mean size of air voids in the concrete cylinder sections was calculated by the method discussed. The influence of CRM on the size of air voids can be observed by comparing the air voids' mean sizes at different CRM percentages, as shown in Figure 11. It can be seen that as the percentage of CRM in the mix increases, the mean size of air voids tends to decrease. For instance, in the 1:3:6 mix with a W/C ratio of 0.4, the air voids mean size is 1.97 mm when there is no CRM (0% CRM), whereas with 15% CRM, it reduces to 1.71 mm. The air void mean size further decreases to 1.55 mm with 25% CRM.

DOI: 10.3217/978-3-99161-057-1-147

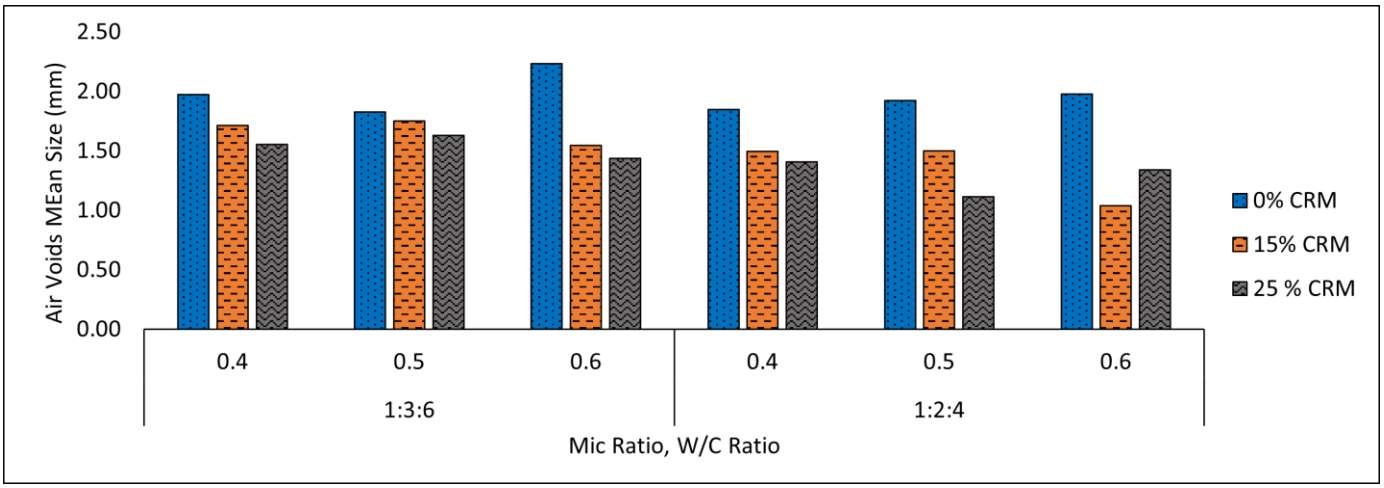

Figure 11. Influence of CRM on the mean size of air voids

4 CONCLUSION

This study explored advanced image processing techniques to investigate the impact of CRM (Silica Fume and Fly Ash) on air void characteristics and aggregate distribution in concrete. Techniques such as the Feret rectangle method and nearest neighbor analysis provided detailed insights into the size, shape, and spatial distribution of aggregates. The following main conclusions can be drawn from the results of the study:

• The analysis of aggregate proportion, quantified through Aggregate Area Ratio (AAR), revealed a close correlation with Aggregate Volume Ratio (AVR) values. This correlation underscores the accuracy and effectiveness of the employed image processing methods in predicting the aggregate proportion.

• The incorporation of CRM led to a notable reduction in both the proportion and size of air voids. This decrease enhances concrete durability by improving resistance to freeze-thaw cycles and reducing cracking risks.

• Increasing CRM content significantly reduces segregation tendencies, leading to a more uniform aggregate distribution across the concrete mix. This improvement is evidenced by lower Cv values, indicating improved homogeneity.

• CRM improved the homogeneity of aggregates by providing more consistent results in terms of aggregate areas, sizes, and roundness, particularly in specimens with higher CRM content. Kurtosis analysis further showed fewer outliers, indicating a more even distribution of aggregates.

• The image processing techniques, including the Feret rectangle method and nearest neighbor analysis, showed an error rate of less than 1.90%, confirming their reliability and accuracy in predicting aggregate and air void properties.

This study primarily addressed rounded and angular aggregates. However, closely positioned elongated or flaky aggregates or irregular shapes aggregates may overlap, potentially leading algorithms to inaccurately identify them as a single aggregate. This could affect the analysis of parameters such as area, length, and roundness. While manual labeling ensures accuracy, it is labor-intensive and subjective, limiting scalability for large-scale or rapid analysis needs. In future work, we plan to use deep learning-based image processing methods, i.e., DeepLabv3+, UNET, and vision transformers, to segment and quantify aggregate and air void characteristics. Additionally, we aim to validate the effect of different CRM ratios on homogeneity by analyzing the distribution of aggregates and air voids at various sections of other structural members in real-world applications.

ACKNOWLEDGMENTS

The authors are thankful to Oslomet University for investigating this research.

FUNDING

This is the part of the Project “Forensic Analysis of Concrete Through Image Processing” FACIP, funded by the EU against The Grant agreement ID: 101153307, https://cordis.europa.eu/project/id/101153307.

REFERENCES

[1] H. Mikul˘ci´c, J. J. Kleme˘s, M. Vujanovi´c, K. Urbaniec, N. Dui´c, Reducing greenhouse gasses emissions by fostering the deployment of alternative raw materials and energy sources in the cleaner cement manufacturing process, Journal of Cleaner Production 136 (2016) 119–132.
[2] S. Vivek, G. Dhinakaran, Durability characteristics of binary blend high-strength scc, Construction and Building Materials 146 (2017) 1–8.
[3] S. S. Nachiar, et al., A review on fly ash cenosphere as a solid waste in concrete application, Materials Today: Proceedings 68 (2022) 2072–2078.
[4] T. Luo, C. Hua, F. Liu, Q. Sun, Y. Yi, X. Pan, Effect of adding solid waste silica fume as a cement paste replacement on the properties of fresh and hardened concrete, case stud. constr. mater., 16 (2022) e01048.
[5] A. I. Laskar, S. Talukdar, Rheological behavior of high-performance concrete with mineral admixtures and their blending, Construction and Building Materials 22 (12) (2008) 2345–2354.
[6] T. Yang, H. Zhu, Z. Zhang, X. Gao, C. Zhang, Q. Wu, Effect of fly ash microsphere on the rheology and microstructure of alkali-activated fly ash/slag pastes, Cement and Concrete Research 109 (2018) 198–207.
[7] D. Jiao, C. Shi, Q. Yuan, X. An, Y. Liu, H. Li, Effect of constituents on rheological properties of fresh concrete-a review, Cement and concrete composites 83 (2017) 146–159.
[8] K. Kim, M. Shin, S. Cha, Combined effects of recycled aggregate and fly ash towards concrete sustainability, Construction and Building Materials 48 (2013) 499–507.
[9] G. Wang, Y. Kong, T. Sun, Z. Shui, Effect of water–binder ratio and fly ash on the homogeneity of concrete, Construction and Building Materials 38 (2013) 1129–1134.
[10] P. Nallathambi, B. Karihaloo, B. Heaton, Effect of specimen and crack sizes, water/cement ratio and coarse aggregate texture upon fracture toughness of concrete, Magazine of concrete research 36 (129) (1984) 227–236.

DOI: 10.3217/978-3-99161-057-1-147

[11] F. de Larrard, A. Belloc, The influence of aggregate on the compressive strength of normal and high-strength concrete, Materials Journal 94 (5) (1997) 417–426.
[12] Standard practice for petrographic examination of hardened concrete (2020).
[13] H. N. Walker, D. S. Lane, P. E. Stutzman, et al., Petrographic methods of examining hardened concrete: A petrographic manual, Tech. rep., United States. Federal Highway Administration. Office of Infrastructure . . . (2006).
[14] J. Elsen, Microscopy of historic mortars—a review, Cement and concrete research 36 (8) (2006) 1416–1424.
[15] P. E. Stutzman, Applications of Scanning Electron Microscopy in Cement and Concrete Petrography, Petrography of Cementitious Materials 1215 (1994) 74.
[16] M. A. Esfahani, M. Kalani, Petrographic analysis method for evaluation and achieving durable hot mix asphalt, Construction and Building Materials 234 (2020) 117408.
[17] C. Koch, K. Georgieva, V. Kasireddy, B. Akinci, P. Fieguth, A review on computer vision-based defect detection and condition assessment of concrete and asphalt civil infrastructure, Advanced Engineering Informatics 29 (2) (2015) 196–210.
[18] C. Fang, S. Labi, Image-processing technology to evaluate static segregation resistance of hardened self-consolidating concrete, Transportation research record 2020 (1) (2007) 1–9.
[19] X. Xu, S. Xu, L. Jin, E. Song, Characteristic analysis of Otsu threshold and its applications, Pattern recognition letters 32 (7) (2011) 956–961.
[20] J. Han, K. Wang, X. Wang, P. J. Monteiro, 2D image analysis method for evaluating coarse aggregate characteristic and distribution in concrete, Construction and building materials 127 (2016) 30–42.
[21] K. Zhang, Z. Zhang, Y. Luo, S. Huang, Accurate detection and evaluation method for aggregate distribution uniformity of asphalt pavement, Construction and Building Materials 152 (2017) 715– 730.
[22] J. Wu, X. Zhou, X. Zeng, Y. Xie, G. Long, R. Dong, H. A. Umar, G. Ma, L. Yao, Effect of aggregate morphology characteristics on the voidage of aggregate loose packing based on 3d discrete element method, Construction and Building Materials 348 (2022) 128598.
[23] S. N. Abbas, M. I. Qureshi, M. K. Alkharisi, M. Alturki, Z. Ahmad, Combined effect of silica fume and various fibers on fresh and hardened properties of concrete incorporating HDPE aggregates, Construction and Building Materials 445 (2024) 137940.
[24] D. G. Daniel, C. L. Lobo, User's Guide to ASTM Specification C 94 on Ready-mixed Concrete, ASTM International, 2005.
[25] A. Committee, Building code requirements for structural concrete (aci 318-08) and commentary, American Concrete Institute, 2008.
[26] AutoCAD software, version 2023. URL https://www.autodesk.com/products/autocad/overview
[27] W. Wang, Image analysis of particles by modified ferret method—best-fit rectangle, Powder Technology 165 (1) (2006) 1–10.